Proceedings of the General Donald R. Keith Memorial Conference
of the Society for Industrial and Systems Engineering,
West Point, New York, USA
April 30, 2015

Decision Support Tool for Designing Niche Small Package Delivery Aerial Vehicles (DST-NSPDAV)

Ashruf Ali, Nathan Ballou, Brad McDougall, and Jorge Luis Valle

George Mason University

Department of Systems Engineering and Operations Research

Email: aali21@gmu.edu , nballou@gmu.edu , bmcdoug2@gmu.edu , jvallera@gmu.edu

Author Note: The authors of this paper are senior systems engineering students from George Mason University's Systems Engineering and Operations Research Department that are concluding their senior capstone design projects.

Abstract: A growing market is the application of multi-rotor vehicles to niche delivery services such as just-in-time spare parts delivery, real-time asset repositioning, rapid food delivery, and remote medical supply delivery. These services are unique in their requirements, meaning there is no single aerial vehicle configuration that is optimal for every scenario. More importantly, these service providers do not have the expertise to design and operate small multi-rotor vehicles that are now feasible due to advances in technology. This is a complex design decision with non-linearities in the design-state-space. This paper presents a decision-support tool to assist small package delivery service providers in configuring the best multi-rotor vehicle for their payload application.

The decision-support tool for the design of multi-rotor small package delivery aerial vehicles (SPDAV) takes inputs such as payload, wind, maximum dimension data, price range, and flight profile, and recommends suitable configurations. A configuration is defined as a frame size and weight, number of rotors and rotor torque, battery (size, voltage, amperage), propeller, and micro-controller. The algorithm used to generate the design-state-space consists of two separate models of multi-rotor aircraft: (1) a power consumption model and (2) a full dynamic flight model. The power consumption model evaluates the steady-state performance of the battery, motor, and propeller combinations at hover, 80%, and full throttle to determine systems that satisfy the users' requirements. A dynamic flight model is then applied to these configurations to further account for environmental factors, airframe aerodynamics, and specific flight profiles

Keywords: Power-Model, Dynamic-Model, Multi-Rotor

1. Context

1.1 Multi-Rotor Aerial Vehicles

Modern day advances in batteries, microcontrollers, and lightweight materials have led the unmanned multi-rotor aerial vehicles market away from being merely hobbyists toys to now mass produced aircraft with commercial applications. Multi-rotors, for the sake of this paper, are rotorcraft with more than two propellers that do not have varying pitch and are capable of vertical takeoff and landing. This allows for easier flight control because movement is achieved by simply deviating the power to propellers, making programmable flight control a viable capability. The reliability and maintainability is also superior to traditional rotorcraft due to the simpler rotor mechanics from less required moving parts. Multi-rotors are relatively small, with size ranging from one to ten feet tip-to-tip, making them more responsive and easier to change direction. Most importantly, multi-rotors are commercially off the shelf available with a wide variety in custom and pre-built configurations. A multi-rotor configuration is defined as a frame size and weight, number of rotors and rotor torque, battery (size, voltage, amperage), propeller, and micro-controller.

1.2 Small Package Delivery

Large companies such as Amazon, Google, DHL, and Dominos have recognized the capability of the multi-rotor aerial vehicles and have invested in straightforward package delivery. With their financial and intellectual resources these companies are positioned to leverage this technology. In addition to package delivery, there exist many other *niche* delivery services such as just-in-time spare parts delivery, real-time asset repositioning, rapid food delivery, and remote medical supply delivery. These services are unique in their requirements, meaning there is no single aerial vehicle configuration that

is optimal for every application. More importantly, these service providers do not have the in-house expertise or financial resources to design and operate small multi-rotor vehicles.

1.3 Design-Engineering Difficulties

Despite being relatively simple in design when compared to other aerial vehicles, the challenge for designing multi-rotors is due to the large amount of possible configurations and the non-linear interactions in the design-space. . Choosing a configuration that meets a set of requirements optimally is not possible without expertise or a decision-support tool.

One of the difficulties incurred during the design of multi-rotors is the non-linearity in the trade-space. For instance, a change to the battery does not mean one can expect some incremental correlated change to the distance capable of being traveled. For example, while evaluating the total payload, one must ensure there is enough power to handle the increased weight. This will then require a battery that is capable of keeping up with the increased need for power. In order to support this larger battery, an adequate frame will be needed. With this now overall increase in total weight one will need more power, and the cycle continues.

1.4 Problem Statement

The advances in multi-rotor aerial vehicle technologies have enabled applications for small package delivery. Unlike the large logistics companies with financial and intellectual resources to design and operate these vehicles from a complex and non-linear design-space, enterprises with niche applications (e.g. asset repositioning, spare parts delivery, rapid food or flower delivery) do not have the expertise to design the optimum vehicle to meet the requirements of their application.

2. Method of Analysis

2.1 Decision-Support Tool Overview

The DST is conducted in two stages – first a power model to identify promising candidates; then a full dynamic model to further characterize the specific performance of these configurations.

For the power model, the user defines a maximum size, cost, minimum distance to travel with full payload, and maximum payload weight. These factors are then put through a simulation that approximates the power draw, motor temperature, hover characteristics, and flight duration. This portion of the simulation searches through a finite list of either currently manufactured multi-rotor configurations or samples permutations of motor, battery, and propeller combinations. Unreasonable configurations (hovering requires greater than 80% throttle, exceeds maximum cost or size, motor temperature at maximum throttle exceeding 80 degrees Celsius.) The remaining configurations are then ranked based on user-defined weights to prioritize models run through the full dynamic simulation.

The full dynamic model takes viable configurations from the power model and subjects them to a more detailed simulation. The model simulates the multi-rotor's performance over a user defined flight path. Maximum flight distance for a given configuration is found by running the simulation multiple times and applying Newton's method to determine the distance corresponding to a battery drain from 80% to 10% to account for battery degradation and provide a cushion of performance safety. The simulation is conducted for a selection of wind profiles and package weights corresponding to user inputs. These results are displayed in a three-dimensional graph that compares wind speed, payload (package) mass, and the delivery distance. This three dimensional graph helps define the endurance-payload-wind tradespace for a given multi-rotor configuration.

After running the full simulation, the output additionally shows a graph where different configurations or pre-assembled multi-rotors are evaluated based on their performance to carry a payload on a distance range. Figure 1 shows an example of a final output with five different multi-rotors performing under different payloads. As it can be seen on the graph, each curve represents how each multi-rotor performs with varying payloads. In order to obtain a performance value, the integral under the curve is calculated (notice that each curve is fitted to a third degree order function to be as accurate as possible) for different ranges of payload to see which configuration would best meet the end user requirements.

Table 1: Performance Values

Model	0 to 2 kg	2 to 5 kg	5 to 8 kg	Cost
HL48	11.889	10.407	0.970	$15,000.00
DJI-S800	6.252	7.238	4.246	$3,399.00
X8-HLM	6.497	0.000	0.000	$2,467.97
OFM-GQ8	8.924	11.684	8.840	$10,299.00
FAE-960H	15.100	9.093	0.000	$9,988.12

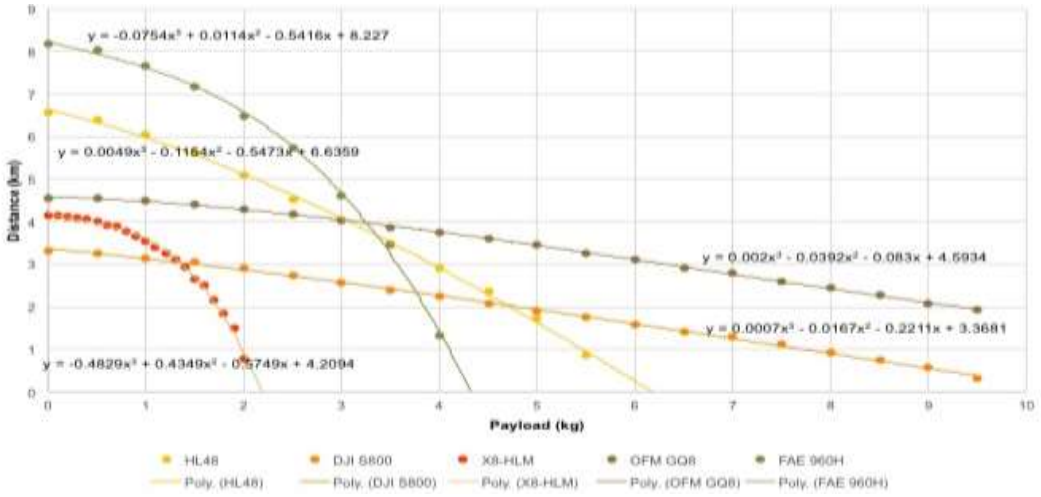

Figure 1. Multi-rotor Performance Curves

2.2 Dynamic Model Coordinate System

The dynamic simulation is a more detailed simulation for highly ranked outputs of the preliminary simulation steps. The simulation models frame aerodynamics; propeller thrust; motor, electronic speed controller, and battery system performance; and inertial response to output a detailed picture of the multi-rotor's performance. This information is used to approximate the flight characteristics of the multi-rotor over a given flight profile, wind, and payload setup.

The dynamic simulation operates in a six degree of freedom environment. The position of the body in space is both defined by translational motion in the x-y-z axis and by Euler angles $\psi - \theta - \phi$, referred to as yaw, pitch, and roll. The simulation defines three coordinate systems in this 6-DoF environment: an inertial North East Down (NED), a body frame, and a geodetic. The inertial frame is fixed on the starting location of the simulated flight profile, and defines the location and orientation in relative space. The body frame is fixed on the multi-rotor's center of gravity. This origin decouples actuation forces and moments and allows for a constant moment of inertia tensor. The locations and orientations of the body and inertial frame are as shown below in Figure 2.

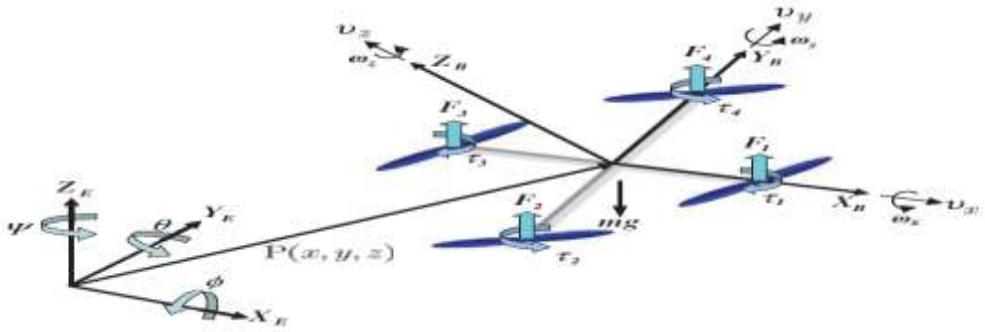

Figure 2. Body and Inertial Frame

Transformation maticies are used to represent translation and rotation in both coordinate systems. Motion in the body frame is transformed through $\psi - \theta - \phi$ rotations as shown in (1). Combining these transformations yeilds the direction cosine matrix H_B^I displayed in (2). For example, velocity measured in the body frame is transformed to the inertial frame as $v_I = H_B^I v_b$. A similar transformation (3) is performed for angular velocities and accelerations where p, q and r are rotational velocities around each translational axis (4). It should be noted that this transformation matrix yields singular

results around $\theta = \frac{\pi}{2}$. We deem this limitation acceptable as small package delivery does not typically encounter such aggressive flight maneuvers. Should such maneuvers be desired, a switch to a quaternion representation could be implemented.

$$H_I^1(\psi) = \begin{bmatrix} \cos\psi & \sin\psi & 0 \\ -\sin\psi & \cos\psi & 0 \\ 0 & 0 & 1 \end{bmatrix}, H_1^2(\theta) = \begin{bmatrix} \cos\theta & 0 & -\sin\theta \\ 0 & 1 & 0 \\ \sin\theta & 0 & \cos\theta \end{bmatrix}, H_2^B(\phi) = \begin{bmatrix} 1 & 0 & 0 \\ 0 & \cos\phi & \sin\phi \\ 0 & -\sin\phi & \cos\phi \end{bmatrix} \quad (1)$$

$$H_B^I(\phi, \theta, \psi) = H_I^1 H_1^2 H_2^B = \begin{bmatrix} \cos\theta\sin\psi & \sin\phi\sin\theta\cos\psi - sin\psi cos\phi & \cos\phi\sin\theta\cos\psi + \sin\phi\sin\psi \\ \cos\theta\sin\psi & \sin\phi\sin\theta\sin\psi + \cos\phi\cos\psi & \cos\phi\sin\theta\cos\psi - \sin\phi\sin\psi \\ -\sin\theta & \sin\phi\cos\theta & \cos\phi\cos\theta \end{bmatrix} \quad (2)$$

$$\begin{bmatrix} p \\ q \\ r \end{bmatrix} = I_{3x3} \begin{bmatrix} \dot{\phi} \\ 0 \\ 0 \end{bmatrix} + H_2^B \begin{bmatrix} 0 \\ \dot{\theta} \\ 0 \end{bmatrix} + H_2^B H_1^2 \begin{bmatrix} 0 \\ 0 \\ \dot{\psi} \end{bmatrix} \quad , \quad L_B^I(\phi, \theta, \psi) = \begin{bmatrix} 1 & \sin\phi\tan\theta & \cos\phi\tan\theta \\ 0 & \cos\phi & -\sin\phi \\ 0 & \sin\phi/\cos\theta & \cos\phi/\cos\theta \end{bmatrix} \quad (3,4)$$

Finally, a geodetic axis is used to more accurately approximate local gravity conditions. Transformations are approximated using the WGS84 standard using the following formula (5).

$$x = (N + h)\cos\phi'\cos\lambda', y = (N + h)\cos\phi'\sin\lambda', z = \left(\left(\frac{b^2}{a^2}\right)N + h\right)\sin\phi', \text{where } N = \frac{a}{\sqrt{1 - e^2 \sin^2\phi}} \quad (5)$$

2.3 Models and Theories Utilized

The simulation is conducted in the Simulink environment to aid accessibility and future customization. The model consists of the following self-contained modules:

2.3.1 Body Geometric and Inertial Calculations

The dynamic simulation begins with the definition of the current vehicle simulation. This definition includes mass, dimensions, and performance properties of the motors, central hub, arms, payload, and propellers. These components are modeled as simple solids to approximate the overall mass, moments of inertia, and geometric conditions. Motors and the central hub are modeled as cylinders and the arms and payload as cuboids. Propellers are represented as thin rectangles for the purpose of these approximations.

The first characteristic of the model approximated is the overall vehicle mass. This is simply the sum of the individual components. This sum is then used to define the center of mass for the representative model. For the purposes of this simulation, the multi-rotor vehicles are assumed to be symmetrical in the vertical and horizontal planes. The following defines the distance from the center of the central cylinder to the center of gravity on the z-axis (6). All component locations are then redefined on the new body origin at this location.

The simple solids model is then used to calculate the overall inertial moments for the vehicle. This involves first calculating the moment of inertia for each individual component, transforming it to be parallel to the main body axis (7) (8), and then using the parallel axis theorem to form the complete moment value (9).

This solids approximation is also used to estimate the surface area for use in drag calculations. For a quadcopter example, the following is the projected side and vertical surface area (10). Lastly, the approximate centroid is calculated (11) to define the point of drag action using the corner points of the approximated multi-rotor shape.

$$G = \frac{n_r\left[m_m\left(\frac{z_a}{2} + \frac{z_m}{2}\right) + m_p\left(\frac{z_a}{2} + z_m + z_s\right)\right] - m_p\left(\frac{z_c}{2} + \frac{z_p}{2}\right)}{m_{tot}} \quad (6)$$

$$I_L = TI_{LR}T^T, \; T = \begin{bmatrix} \cos\theta & \sin\theta & 0 \\ -\sin\theta & \cos\theta & 0 \\ 0 & 0 & 1 \end{bmatrix}, \quad I_O = I_L + md^2 \quad (7,8,9)$$

$$A_X = A_Y = 2r_c h_c + 2l_a h_a + 4r_m h_m + l_p h_p \quad A_Z = w_p l_p + 4l_a w_a + 4\pi r_m^2 \quad , \quad C = \frac{1}{k}\sum_i^k x_i \quad (10,11)$$

2.3.2 Atmospheric Model

The atmospheric model is the MATLAB aerospace toolbox implementation of the ISA atmospheric model for altitudes below 20000 m.

2.3.3 Gravity Model

The Gravitational Model (12) uses the second order EGM96 model for gravitational potential (NIMA, 2000) using the geodetic coordinate system.

$$V = \frac{G}{r}\left[1 + \sum_{n=2}^{n_{max}} \sum_{m=0}^{n} \left(\frac{a}{r}\right)^n \bar{P}_{nm}\, sin(\phi')\, (\bar{C}_{nm} \cos m\lambda + \bar{S}_{nm} \sin m\lambda)\right] \quad (12)$$

2.3.4 Electrical System Model

The electrical system model consists of the motor model, the battery model, and the throttle curve model. These models are necessarily coupled as motor current draw changes the battery voltage output, which then changes the motor current draw etc. At each time step, the systems are modeled until they converge on a value (within 0.1%).

2.3.5 Motor Model

The motor model approximates the performance of a brushless dc (BLDC) electric motor. These motors were chosen for their high power to weight ratios, efficiency, and low maintenance requirements and are standard components in current multi-rotor UAVs. The model is based on Kirchhoff's voltage law (13) and Newton's second law (14) as described by Movellan (2010) with some alterations.

The inductance of the motor is very difficult to measure and is, in any case, very small for this type of motor, so it will be neglected (15). The load torque has quadratic dependence on motor and propeller angular velocity, so $\tau_{load} = d\Omega^2$ (16).

The BLDC motors used in this application reach steady state very quickly due to low inductance and rotational inertia. The time constant for no load is approximately 0.03 s, significantly smaller than the simulation step time. The model is therefore further simplified to assume steady state operation (17). Rearranging shows the voltage required to reach a desired motor speed (18).

$$V = L\frac{dI}{dt} + RI + K\Omega \quad , \quad J\frac{d\Omega}{dt} = KI - \lambda\Omega - \tau_{load} \quad (13,14)$$

$$V = RI + K\Omega \quad , \quad J\dot{\Omega} = -\frac{K^2}{R}\Omega - d\Omega^2 + \frac{K}{R}V \quad (15,16)$$

$$\Omega^2 + \frac{K^2}{Rd}\Omega - \frac{K}{Rd}V = 0 \quad , \quad V = \frac{Rd}{K}\Omega^2 + K\Omega \quad (17,18)$$

2.3.6 Battery Model

The battery model approximates the non-linear power draw of a lithium polymer battery (LiPoly). This battery type is chosen for its high power density. This BLDC and LiPoly setup is standard for commercial multi-rotor designs. This model is currently implemented using the simMechanics Simulink block-set, but a more detailed representation will be integrated into future simulation iterations.

2.3.7 Throttle Curve Model

The throttle curve model approximates the electronic speed controller response to a given controller output. This is in the form of a curve match based on reference ESC data.

2.3.8 Aerodynamic Model

The aerodynamic model uses the projected surface area calculated before as described by Moyano (2013) to calculate the airframe drag. The general form of the drag equation (19) is modified for this purpose as below. This general form is first modified to take into account the varying surface area and drag coefficient based on relative orientation (20). We can therefore calculate the individual components of the drag as follows (24).

The area function is approximated based on the sideslip and angle of attack of the vehicle. This simplification is used due to the relatively crude geometric representation and computational difficulties of estimating instantaneous frontal surface area. We therefore approximate the area as a ratio of the frontal and side areas (22).

The C_d value is much more difficult to approximate. An accurate calculation would involve a CFD analysis on a specific frame geometry and propeller wake properties - an analysis far beyond the scope of this simulation. We therefore estimate the drag coefficient as a function between a max and min C_d value based on experimental data.

Lastly, the relative centroid based on airflow direction must be calculated to complete the aerodynamic force characterization. The drag moment is approximated in a manner similar to the frontal surface area (23)(24).

$$F_d = \frac{1}{2} C_d \rho A v^2 \quad , \quad F_d = \frac{1}{2} \rho C_d(\beta_{SS}, \alpha) A(\beta_{SS}, \alpha) V_\infty^2 \quad , \quad F_d = \begin{cases} F_{dx} = F_d \cos\beta_{SS} \cos\alpha \\ F_{dy} = F_d \sin\beta_{ss} \cos\alpha \\ F_{dz} = F_d \sin\alpha \end{cases} \qquad (19,20,21)$$

$$A \cong A_x \cos\beta_{SS} \cos\alpha + A_y \sin\beta_{SS} \cos\alpha + A_z \sin\alpha \qquad (22)$$

$$M_d = r_d(\beta_{ss}, \alpha) \times F_d \quad M_d = r_d(\beta_{SS}, \alpha) \sin\theta_d F_d \quad , \quad r_d \cong r_{dx} \cos\beta_{SS} \cos\alpha + r_{dy} \sin\beta_{SS} \cos\alpha + r_{dz} \sin\alpha \qquad (23,24)$$

The simplifications above may result in significant deviations from experimental data collected in the validation stage. Further work may be needed to more accurately approximate this phenomenon.

2.3.9 Propeller Model

The propeller model is the most complex portion of the simulation. A combination of Blade Element Theory (BET) and Momentum Theory (MT) are used to model the rotor performance characteristics. This method of analysis was chosen as a balance of computational intensity and accuracy, and has been used frequently in helicopter and other multi-rotor studies. This model is based heavily on the work of Martinez (2007) and Mansson (2014).

3. References

Kim, J. (2009, September). Accurate Modeling and Robust Hover Control for a Quad-rotor VTOL Aircraft.

Mansson, C. (2014, June). Model-based Design Development and Control of a Wind Resistant Multirotor UAV.

Fresk, E. (2006, July). Full Quaternion Based Attitude Control for a Quadrotor.

NIMA. (2000, January) Department of Defense World Geodetic System 1984.

Movellan, J.R..(2010). DC Motors, Machine Perception Laboratory, University of California.

Moyano, J. (2013). Quadrotor UAV for wind profile characterization.

Martinez, V. (2007, September). Modeling of the Flight Dynamics of a Quadrotor Helicopter.

Leishman, J.G.. (2002). Principles of Helicopter Aerodynamics 2nd Edition.

Prouty, R.W.. (1990). Helicopter Performance, Stability and Control.

Pounds, P. (2006, December). Modelling and Control of a Quad-rotor Robot.

Bresciani. T. (2008). Modeling, Identification and Control of a Quadrotor Helicopter.

Banura, M & Mahony, R. (2012, December). Nonlinear Dynamic Modeling for High Performance Control of a Quadcopter.

Capello, E. (2012, October). Mini Quadrotor UAV: Design and Experiment.

Latorre, E. (2011, June). Propulsion System Optimization for an Unmanned Lightweight Quadrotor.

Tesfaye. R. (2012, December). Modeling and Control of a Quad-rotor Unmanned Aerial Vehicle at Hovering Position.